Received ; | Revised ; | Accepted

DOI: xxx/xxxx

ARTICLE TYPE

Study on Bifurcation Analysis and Takagi-Sugeno Fuzzy Sampled-Data Stabilization of PMSM Systems †

R. Vadivel[1] | Sabarathinam Srinivasan[2] | Yongbao Wu*[3] | Nallappan Gunasekaran*[4]

[1]Department of Mathematics, Faculty of Science and Technology, Phuket Rajabhat University, Phuket-83000, Thailand.
[2]Centre for Nonlinear Dynamics, School of Physics, Bharathidasan University, Tiruchirappalli, Tamil Nadu, India.
[3]School of Mathematics and Statistics, Northwestern Polytechnical University, Xi'an 710129, China; MIIT Key Laboratory of Dynamics and Control of Complex Systems, Xi'an 710072, China.
[4]Computational Intelligence Laboratory, Toyota Technological Institute, Nagoya, 468-8511, Japan.

Correspondence
*Nallappan Gunasekaran and Yongbao Wu
Email: gunasmaths@gmail.com (N. Gunasekaran),
yongbaowu199211@163.com (Y. Wu)

Abstract

The bifurcation, stability and stabilization analysis of permanent magnet synchronous motor (PMSM) systems are investigated in this paper. To begin, a new class of delay-dependent sufficient conditions is suggested with respect to the information of the membership function, a relevant Lyapunov-Krasovskii functional (LKF), and the overall information connected with the real sampling pattern, so that the fuzzy system is ensured to be stable with a weighted dissipativity efficiency. Second, sampled-data control is intended to stabilize the Takagi-Sugeno (T-S) fuzzy system with specified integral inequalities based on the obtained results. The required conditions are stated in terms of the feasibility of linear matrix inequalities (LMIs) under the dissipativity output index, and can readily be verified by MATLAB toolbox. Finally, verification examples are contributed to demonstrated the efficacy of the techniques established in this paper.

KEYWORDS:
Bifurcation analysis, Dissipativity, Lyapunov method, Linear matrix inequality, Sampled-data control, Takagi-Sugeno fuzzy system.

MSC CLASSIFICATION:
34D20 ; 34A07; 34C23; 37L30 ; 93D20.

1 | INTRODUCTION

Due to their simple design, high performance, low manufacturing cost, high power density, and strong torque-to-inertia ratio, permanent magnet synchronous motor (PMSM) are widely used in a variety of industrial fields[1,2,3]. PMSM exhibit complex behaviors such as Hopf bifurcations, limit cycles, and even chaos because they are nonlinear, multivariable, and tightly coupled[1]. In addition, PMSM behavior in an industrial environment can be affected by many uncertainties, including unknown system parameters, frictional forces, external load disturbances, and unmodeled uncertainties. These uncertainties can significantly reduce the performance quality of PMSM systems in[4].

On the other hand, both stability analysis and stabilization of Takagi-Sugeno (T-S) fuzzy model's have received a plenty of interest in[5]. The T-S fuzzy model in[6], which represents a highly nonlinear dynamic system with fuzzy mixing structure of local linear sub-models. Owing to its particular advantages that can be closely compared to any high-precision nonlinear system, the technique has been recognized as major fundamental procedures to dealing with nonlinear control systems. As a result, in recent years, a significant number of theoretical findings and functional implementations of T-S fuzzy systems have been published in[7,8]. For example, the T-S fuzzy complex dynamical networks[9,10] have solved the synchronization analysis in view of the

† vadivelsr@yahoo.com (R. Vadivel), saba.cnld@gmail.com (Sabarathinam Srinivasan)

finite-time approach. Recently, in [11,12] sampled-data stabilization for T-S fuzzy systems have been studied. In [13,14] the authors extensively analyzed the exponential time-varying gains in the sense of fault tolerant sampled-data fuzzy observer. The majority of real-world systems include a nonlinear system's stability analysis. Furthermore, since time delay is inherent in many practical applications such as control systems, state-feedback, and actuator dynamics, it can degrade control efficiency [15,16,17]. The topic of dissipativity analysis is of primary importance in the design of PMSM model because it ensures that dynamical systems performance and satisfactory response [18]. So far, several theoretical achievements for extended dissipative analysis related to T-S fuzzy structures with or without time delays have been elaborated in the literature.

The sampled-data control (SDC) technique has recently been the hottest topic of dynamical systems. It is a sampling process in which the control signal is kept constant during the sampling time period and only allowed to adjust at the time of sampling. Furthermore, in SDC systems, selecting the right sample space is crucial for planning suitable controllers. Many researchers have recently analyzed into the standard model's case. As a result of its use in a variety of functional approaches, time-varying sampling is commonly used. The SDC technique has been recognized as a useful mechanism for controlling T-S fuzzy methods in [19,20,21,22]. However, a large variety of results have been stated on SDC system. For example, secure communication [23], Chua's circuit [24], wind-turbine system [25], and autonomous surface vehicle systems [26] in practice. Fuzzy sampled-data stabilization, which only samples at the sampling instant and does not require signals to be sent continuously, has dramatically reduced the number of transmitted signals. The principle objective of sampled-data stabilization is to acquire a relatively larger sampling interval such that the system is stable [27,28]. Many interesting results related for sampled-data stabilization T-S fuzzy systems have been reported in the literature. Some examples are given below. In [29], the authors have been investigated for the stabilization of T-S fuzzy systems with actuator failures and sampled-data fuzzy stabilization. The literature [30] developed a nonlinear delayed distributed parameter systems by using sampled-data fuzzy stabilization. In [31], the researchers discussed the issue of sampled-data synchronization of T-S fuzzy reaction-diffusion neural networks.

Furthermore, dissipativity is a general principle of passivity, which is significant in both theoretical and functional aspects of mechanism and control theory [32,33]. The theory of passivity is a generalization of dissipativity in electrical networks and other dynamical systems that dissipate energy in some abstract context. Dissipativity theory is a crucial method for studying the consistency and passivity of control systems [34,35] provides a framework for control system design and analysis using an input–output description based on energy-related considerations. As a result, it is assumed that when approximating a high-order T–S fuzzy system with reduced-order models, dissipativity has been maintained. By utilizing T-S fuzzy model, the researchers in [36] explored the sampled-data control performance for nonlinear systems using passivity and passification approaches. However, the results reported in [37,38,39] cannot have a merit because those obtained results have not focused on exogenous disturbances ($\mathcal{L}_2$). Furthermore, when considering exogenous disturbances, the system's output analysis is an important problem for sampled-data T-S fuzzy systems, since it can be considered whether the system can accommodate a certain amount of chaos. When exogenous disruptions are considered, the issue of stabilization analysis and control synthesis becomes more complex and difficult. However, the problems of stability analysis and weighted dissipativity efficiency for sampled-data T-S fuzzy PMSM system have not been studied up to this stage. This structural model is difficult to attain, but it is of considerable importance and attention, which motivates us to conduct this research.

With the above in mind, the problem of extended dissipative analysis of sampled-data fuzzy PMSM system using the enhanced integral inequality methodology is investigated in this paper. As a result, in this note, LKF is constructed with the information of sampling delay to ensure the extended dissipative conditons are provided. To do this, numerical examples are addressed to manifest the superiority of the developed stability criteria. The following key points represent the highlights and main contributions of this paper:

(H1) To stabilize a complex PMSM system, we will use the sampled-data controller.

(H2) The sampled-data method is investigated using the T-S fuzzy model, taking into account dissipativity efficiency, actual sampling pattern, and the development of a delay-dependent criterion, such that the considered system is extended dissipative.

(H3) By using the desired controller scheme and selecting a proper Lyapunov–Krasovskii functional, which can fully capture the information of sampling.

(H4) All of the necessary conditions are represented as LMIs, which can be solved quickly with MATLAB tools. With these conditions, the gain matrices are calculated.

(H5) Compared with the stability criteria in [28], [29], the obtained stability results in this paper, improve control execution of the system and loosen up the limitations on the system by utilizing our SDC strategy and has been illustrated in the simulation results section.

Notations: Throughout the paper, $\mathbb{R}^n$ denotes the n dimensional Euclidean space and $\mathbb{R}^{m\times n}$ is the set of all $m\times n$ real matrices, respectively. "*" indicates as symmetric block matrix.

2 | CASE STUDY FOR PERMANENT MAGNET SYNCHRONOUS MOTOR (PMSM):

AC induction motors actually power the majority of pumps and fans used in industrial and commercial applications. 'ACIM" stands for alternating current induction motor, and it is an asynchronous motor that turns the rotor using electric current. Electric current in the rotor generates torque. The magnetic field of the stator windings generates electromagnetic induction, which generates the electric current. The rotor of an ACIM rotates at a slower rate than the magnetic field. A permanent magnet synchronous motor, or PMSM, uses magnets to drive the rotor, which spins at the same speed as the PMSM's internal rotating magnetic field in[3].

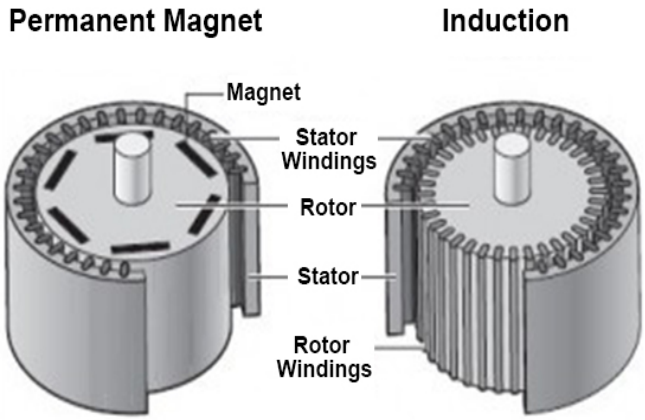

FIGURE 1 AC Induction Motors and Permanent Magnet Synchronous Motors in[3].

Now, consider the voltage conditions of a PMSM's in a mn-outline, as seen in[40], and the following differential equation governs the mathematical model:

$$\begin{aligned} v_n &= r_s i_n + L_n \dot{i}_n + \omega_s L_m i_m + \omega_s \lambda_q \\ v_m &= r_s i_m + L_m \dot{i}_m - \omega_s L_m i_m, \end{aligned} \tag{1}$$

where v_m and v_n represented as mn-frame voltages and currents, i_m and i_n denoted as mn-frame currents, L_m and L_n denote outline inductances, and r_s is winding resistance. ω_s denotes electrical rotor speed, and λ_q denotes the flux connection constructed by permanent magnet.

The electromagnetic torque produced by the PMSMs is as follows:

$$T_e = \left(\frac{3}{2}\right)\left(\frac{P}{2}\right)[\lambda_q i_n + (L_n - L_m) i_n i_m]. \tag{2}$$

A PMSM's mechanical equation is:

$$T_e = J\left(\frac{2}{P}\right)\dot{\omega}_s + B\left(\frac{2}{P}\right)\omega_s + T_L, \tag{3}$$

where J denotes inertia and B denotes the PMSM's damping coefficient, respectively. The input torque is denoted by T_L and P indicated as magnetic pole number. In order to make the better controller, we usually define the m-axis current to zero. The electromagnetic torque of PMSM can thus be precisely limited by tuning the n-axis present.

TABLE 1 PMSM Parameters

Symbols	Value	Unit
r_s	2.87	Ω
L_m	0.0085	H
L_n	0.0085	H
λ_q	0.175	Wb
J	0.008	$kg.m^2$
B	0.001	$kg.m^2/s$
P	4	

The n-axis inductance in the PMSM architecture is similar to the m-axis inductance ($L_n \cong L_m$). The electromagnetic torque in (2) can be reduced to the following:

$$T_e = \left(\frac{3}{2}\right)\left(\frac{P}{2}\right)\lambda_q i_n. \tag{4}$$

The dimensionless mathematical model of PMSM is given in[1]:

$$\begin{aligned}
\dot{i}_n &= \frac{1}{L_n}\left(v_n - r_s i_n - \omega_s L_m i_m - \omega_s \lambda_q\right)\\
\dot{i}_m &= \frac{1}{L_m}\left(v_m - r_s i_m + \omega_s L_n i_n\right)\\
\dot{\omega}_s &= \frac{1}{J}\left[\frac{P}{2}(T_e - T_L) - B\omega_s\right]\\
&= \left(\frac{3P^2}{8J}\lambda_q i_n - \frac{B}{J}\omega_s - \frac{P}{2J}T_L\right).
\end{aligned} \tag{5}$$

3 | DYNAMICAL ANALYSIS

For numerical analysis, we consider (5) in the following system parameter values which is tabulated in TABLE 2. For specific

TABLE 2 Numerical calculation parameters of (5).

R	9 ω
L_m / L_n	34.5 mH / 24.5 mH
λ_q/J	0.00175 / 0.08
B / P	0.001 / 2.0031
T_L / v_n /v_m	1.5 / 1.0 / 3.0

ranges of parameter values, the stated system exhibits chaotic oscillations as shown in FIGURE 2 . Notice that the first and third variables such as i_n, ω_s are linearly/exponentially increased with its amplitude. But the time series of i_n, i_m are in chaotic oscillations which are shown in FIGURE 2 (a,c) inset of (a). Moreover, the variable i_m, has sustained chaotic oscillations which are shown in FIGURE 2 (b). FIGURE 2 has plotted after removing 1×10^3 of transient data points which is shown that the asymptotic behaviour of the system has chaotic oscillation.

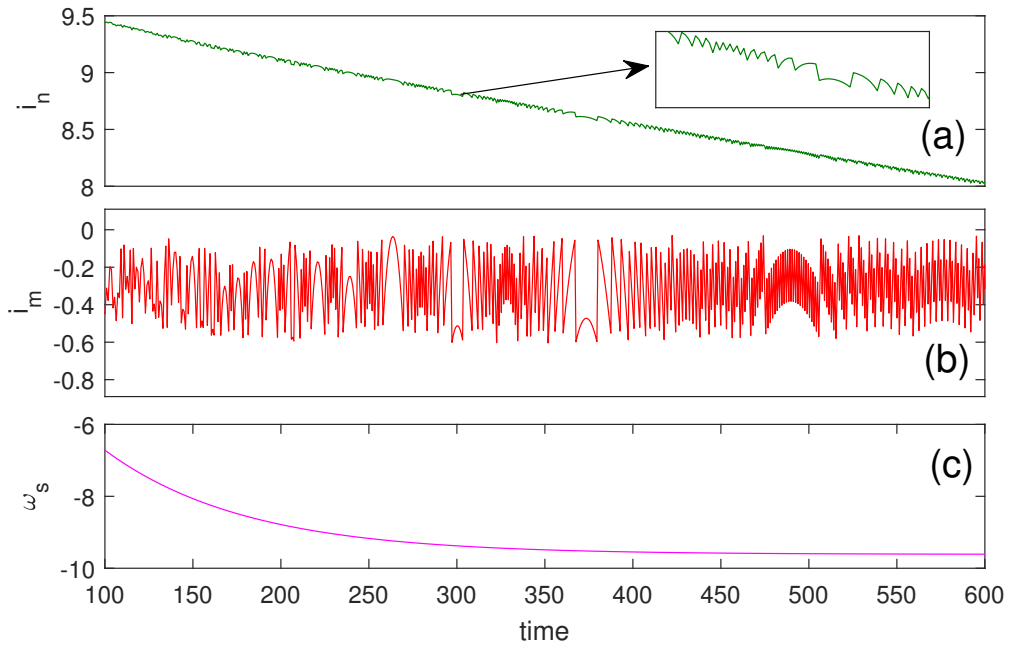

FIGURE 2 Numerically computed time trajectories of (5) in the i_n, i_m and ω_s variables. Notice that variables i_n and ω_s are looking exponential form with respect to time but it evolves with stochastic nature (inset).

3.1 | Bifurcation Analysis

The bifurcation analysis carried out to understand the global and local dynamics of the proposed system (5). FIGURE 3 shows (a) Lyapunov exponent spectrum and its corresponding (b) bifurcation diagram with respect to the co-efficient L_n. For calculation of Lyapunov exponent (It quantitatively estimates the rate of separation of infinitesimally closed orbits) is described as:

$$\lambda = \lim_{t\to\infty} \lim_{|\delta \mathbf{Z}_0|\to 0} \frac{1}{t} \ln \frac{|\delta \mathbf{Z}(t)|}{|\delta \mathbf{Z}_0|} \tag{6}$$

$\delta \mathbf{Z}_0$ denotes the initial separation of two nearby trajectories in the phase space. It actually provides the divergence rate. The average divergence rate after t^{th} iterations are defined as, $|\delta \mathbf{Z}(t)| \approx e^{\lambda t}|\delta \mathbf{Z}_0|$ and Lyapunov exponent indicated as λ. In general, the rate of separation varied for different orientations of initial detachment vectors. Results, the Lyapunov exponent has an equal number of dimensions of the phase space. A positive maximal Lyapunov exponent is used as a piece of evidence that the system is chaotic (provided some other conditions are met, e.g., phase space compactness). FIGURE 3 (a) shown the maximal Lyapunov exponent with respect to the state variable L_n. Notice that the positive value regime of Lyapunov exponent shows the occurrence of the chaotic oscillations in a wide range of parameter province. Similarly it reflect in the bifurcation diagram 3 (b). For the bifurcation plot (FIGURE 3 (b)), the maximal peak amplitude of the variable i_m considered with the removal of transients.

For getting better clarity of the existence of chaotic attractor in the other parameter regimes, bifurcation analysis was carried out for the system by changing another control parameters of the proposed system (5). FIGURE 4 (a,b) shows the bifurcation diagram of R_s and L_m with respect to the state variable $|i_m|$. The chaotic oscillation regimes were identified from the bifurcation plots of $R_s \in (0, 0.2)$ (FIGURE 4 (a)) and $L_m \in (0, 8)$ (FIGURE 4 (b)) with the densely random dots. The rest of the system parameters are fixed as per Table 2. Moreover, the Lyapunov exponent spectrum can be plotted in these bifurcation diagrams for the sake of simplicity those plots are avoided here.

3.2 | Effect of Initial Conditions

The bifurcation analysis proves, the presence of chaotic oscillations in a wide range of system parameter as well as the various parameters in the proposed system (5). In this section, the sensitivity analysis performed to know the basin of the system state

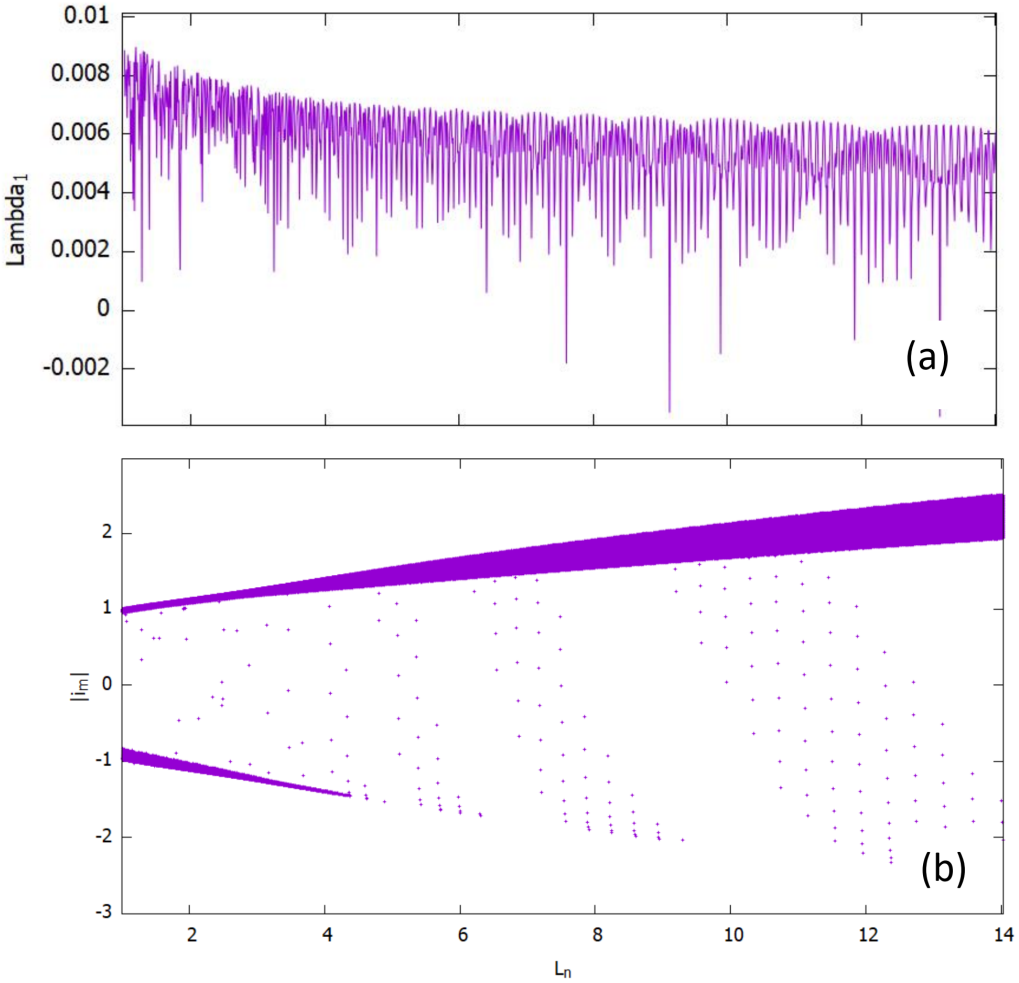

FIGURE 3 (a) Maximal Lyapunov exponent spectra in the $L_n - \lambda_1$ plane and its corresponding; (b) Bifurcation diagram in the $L_n - |i_m|$ plane.

space coordinates. For that, the dynamics (chaotic regimes) of the system is investigated with the different sets of initial conditions (i_n, i_m, w_s) scanning with fixed system parameters. FIGURE 5 exhibits the maximum peak amplitude of the state variable $i_m(i.e, |i_m|)$ with respect of initial conditions (a)i_n , (b) i_m and (c) w_s planes. The system parameters are fixed as the system exhibits chaotic oscillations (Table-II). From this initial condition scanning (basin) diagram symmetry exists only by varying the initial condition i_n (mirror image exists).

The chaotic oscillations are getting larger when the absolute values of initial conditions are in higher values in magnitude. The bounded chaotic attractor is getting smaller in size when the initial conditions are picked up near to zero values. Particularly. near to the regime of trivial equilibrium points, i.e, $(i_n, i_m, w_s)^*$ =(0,0,0) the system has no oscillation. The system has a symmetric nature of oscillation in the $i_n *$ initial condition scanning. The rest of the initial conditions plot i.e, i_m and w_s has an asymmetry nature. From this basin study, the system exhibits a wide range of chaotic oscillations in its basin.

3.3 | Chaos confirmation: 0-1 Test

Using the '0-1' measure, the time series data of i_m is considered for the validation of the chaotic oscillation. Gottwald *etal* suggested determining whether a time series is chaotic or sporadic by measuring the asymptotic rate of growth K (periodic $K = 0$ and chaotic $K = 1$). The state portrait of transnational coefficients p, q confirms the time series' existence in half (smooth:

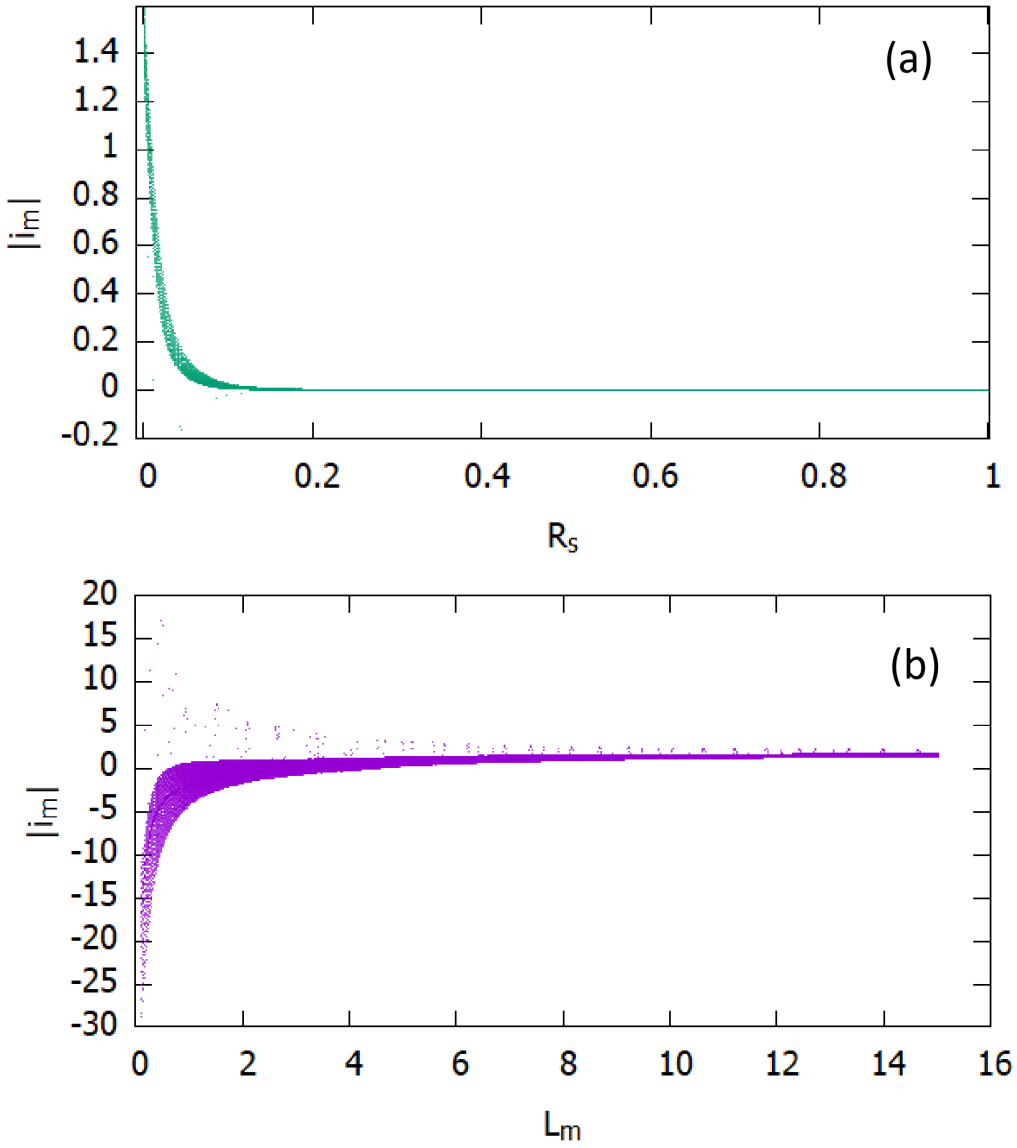

FIGURE 4 (a) Bifurcation diagram in the $R_s - |i_m|$ plane and (b) $L_m - |i_m|$ plane.

periodic, random walk: chaotic). The time series (*FIGURE* 6 (*a*)) is considered has 2×10^4 data length. The approximation is performed with 0.01 step iterations. The genomics components $p - q$ visualize the Brownian motion and partly affirm the chaotic motion, as seen in FIGURE 6 b. The normalized variance $M(n)$ computed from the translation components to find the diffusive behavior of the given time series (for periodic, $M(n)$ is bounded; for chaotic, it linearly increases with time) is shown in FIGURE 6 c. The asymptotic rates of growth are seen in FIGURE 6 (d) , which settles about 1 (we obtain K =0.9941 *sim* 1), confirming the existence of chaos in the specified i_m time sequence.

To ensure that the current monitoring error merges to zero, the state variables are described as follows:

$$\delta_1 = \int [r(t) - z(t)]dt \;\Rightarrow\; z(t) = \omega_s, \tag{7}$$

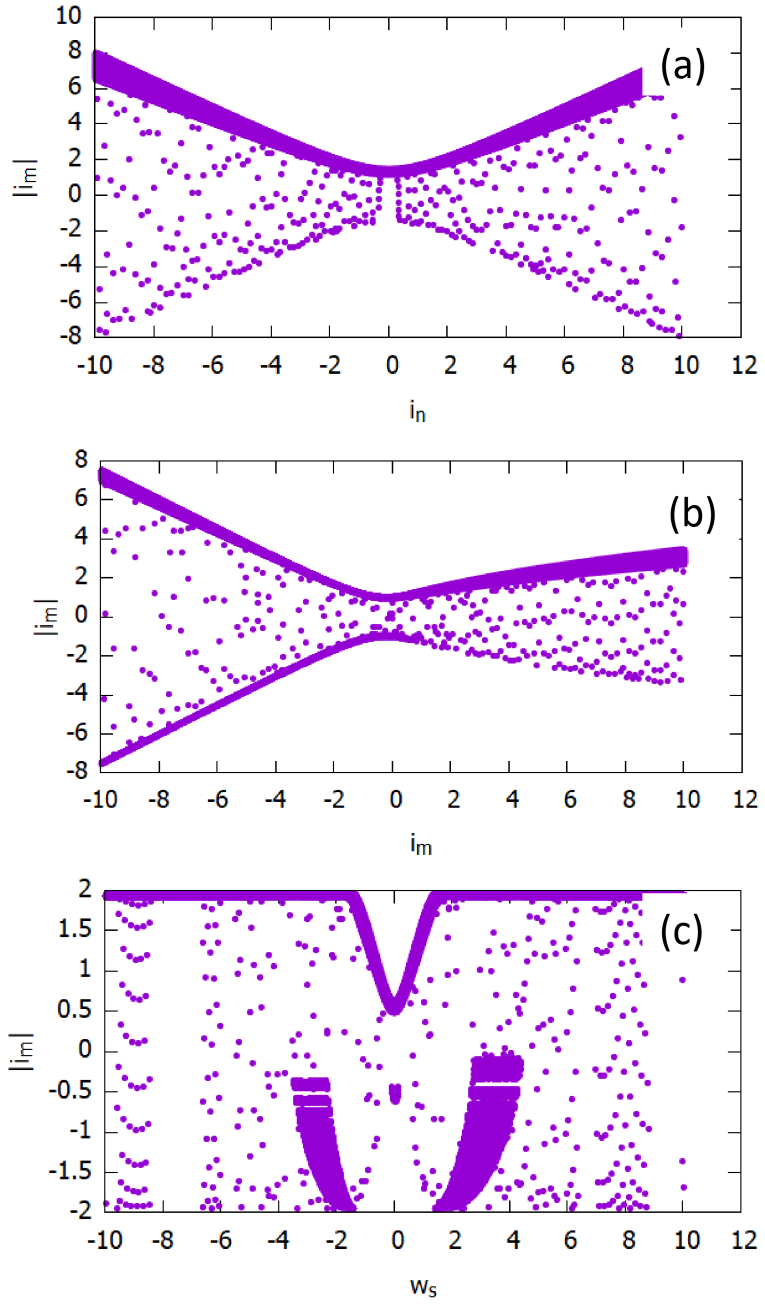

FIGURE 5 Initial conditions (IC) scanning with respect to the maximum peak amplitude of the state variable $|i_m|$. (a) IC: $i_n * -|i_m|$ plane (b) IC: $i_m * -|i_m|$ plane and (c) IC: $w_s * -|i_m|$ plane.

where $r(t)$ is the target value of ω_s. With (1)-(5), the PMSM's state equations can be defined as follows:

$$\begin{bmatrix} \dot{\omega}_s \\ \dot{i}_n \\ \dot{i}_m \\ \dot{\delta}_1 \end{bmatrix} = \begin{bmatrix} -\frac{B}{J} & \frac{3P^2}{8J}\lambda_q & 0 & 0 \\ -\frac{\lambda_q}{L_n} & -\frac{r_s}{L_n} & -\frac{L_m}{L_n}\omega_s & 0 \\ 0 & \frac{L_n}{L_m}\omega_s & -\frac{r_s}{L_m} & 0 \\ -1 & 0 & 0 & 0 \end{bmatrix} \begin{bmatrix} \omega_s \\ i_n \\ i_m \\ \delta_1 \end{bmatrix} + \begin{bmatrix} 0 & 0 \\ \frac{1}{L_n} & 0 \\ 0 & \frac{1}{L_m} \\ 0 & 0 \end{bmatrix} \begin{bmatrix} v_n \\ v_m \end{bmatrix} + \begin{bmatrix} -\frac{PT_l}{2J} \\ 0 \\ 0 \\ u_1 \end{bmatrix}$$

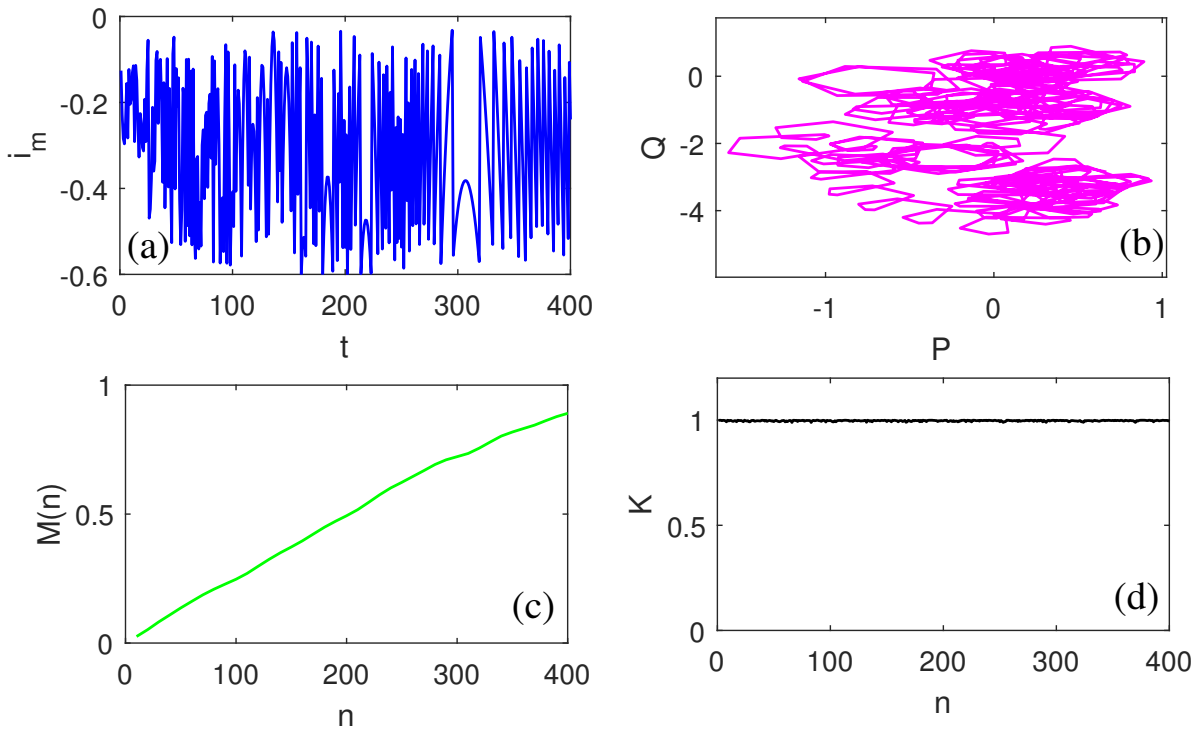

FIGURE 6 The 0-1 test: (a) time series data of i_m, (b) phase portraits of translational components in the $(p-q)$ plane; (c) displacement $M(n)$; (d) asymptotic growth rate: K.

$$\dot{x}(t) = A(x(t)) + Bu(t) + \lambda(t), \tag{8}$$

where

$$A(x(t)) = \begin{bmatrix} -\frac{B}{J} & \frac{3P^2}{8J}\lambda_q & 0 & 0 \\ -\frac{\lambda_q}{L_n} & -\frac{r_s}{L_n} & -\frac{L_m}{L_n}\omega_s & 0 \\ 0 & \frac{L_n}{L_m}\omega_s & -\frac{r_s}{L_m} & 0 \\ -1 & 0 & 0 & 0 \end{bmatrix}, \; B = \begin{bmatrix} 0 & 0 \\ \frac{1}{L_n} & 0 \\ 0 & \frac{1}{L_m} \\ 0 & 0 \end{bmatrix},$$

and $\lambda(t)$ represents the PMSM system's disturbance. The disturbance are defined as follows:

$$\lambda(t) = B_w w(t), \; B_w = \begin{bmatrix} -\frac{P}{2J} & 0 & 0 & 0 \\ 0 & 0 & 0 & 0 \\ 0 & 0 & 0 & 0 \\ 0 & 0 & 0 & 1 \end{bmatrix}, \; w(t) = \begin{bmatrix} T_I \\ 0 \\ 0 \\ u_1 \end{bmatrix},$$

The disturbance is designated as $w(t)$ in the above-mentioned device framework. The PMSM model's performance is as follows:

$$z(t) = \begin{bmatrix} 1 & 0 & 0 & 0 \end{bmatrix} \begin{bmatrix} \omega_s \\ i_n \\ i_m \\ \delta_1 \end{bmatrix} = Cx(t). \tag{9}$$

4 | T-S FUZZY MODEL

Consider a family of T-S fuzzy systems resulting from a nonlinear system
Plant Rule i : **IF** $\tilde{\tilde{\varphi}}_1(t)$ is M_{i1}, $\tilde{\tilde{\varphi}}_2(t)$ is M_{i2}, $\cdots$, and $\tilde{\tilde{\varphi}}_p(t)$ is M_{ip},
THEN

$$\begin{aligned} \dot{x}(t) &= A_i x(t) + B_i u(t) + B_w w(t) \\ z(t) &= C_i x(t), \end{aligned} \tag{10}$$

where

$$A_i = \begin{bmatrix} -\frac{B}{J} & \frac{3P^2}{8J}\lambda_q & 0 & 0 \\ -\frac{\lambda_q}{L_n} & -\frac{r_s}{L_n} & -\frac{L_m}{L_n}d_i & 0 \\ 0 & \frac{L_n}{L_m}d_i & -\frac{r_s}{L_m} & 0 \\ -1 & 0 & 0 & 0 \end{bmatrix}, \; B_i = \begin{bmatrix} 0 & 0 \\ \frac{1}{L_n} & 0 \\ 0 & \frac{1}{L_m} \\ 0 & 0 \end{bmatrix}, \; B_w = \begin{bmatrix} -\frac{P}{2J} & 0 & 0 & 0 \\ 0 & 0 & 0 & 0 \\ 0 & 0 & 0 & 0 \\ 0 & 0 & 0 & 1 \end{bmatrix},$$
$$C_i = \begin{bmatrix} 1 & 0 & 0 & 0 \end{bmatrix}, i = 1, 2$$

where $\tilde{\tilde{\varphi}}_i(t), i \in \mathcal{I} \triangleq \{1, 2, ..., p\}$ are the premises variables; r stated number of fuzzy rules; M_{il}, $l = 1, 2, ..., p$ is the fuzzy sets; $x(t) \in \mathbb{R}^n, u(t) \in \mathbb{R}^m$, and $w(t) \in \mathbb{R}^p$ indicated as state vector, control input, and disturbance input which belongs to $\mathcal{L}_2[0, \infty)$ respectively; $z(t) \in \mathbb{R}^q$ means the output. The system dynamics are described by

$$\begin{aligned} \dot{x}(t) &= \sum_{i=1}^{r} \lambda_i(\tilde{\tilde{\varphi}}(t))\big[A_i x(t) + B_i u(t) + B_w w(t)\big], \\ z(t) &= \sum_{i=1}^{r} \lambda_i(\tilde{\varphi}(t)) C_i x(t), i \in \mathcal{I} \end{aligned} \tag{11}$$

where

$$\lambda_i(\tilde{\varphi}(t)) = \frac{\beta_i(\tilde{\varphi}(t))}{\sum_{i=1}^{r} \beta_i(\tilde{\varphi}(t))}, \; \beta_i(\tilde{\varphi}(t)) = \prod_{j=1}^{r} M_{ij}(\tilde{\varphi}_j(t)),$$

and $M_{ij}(.)$ is the grade membership function of $(\tilde{\varphi}_j(t))$ in M_{ij}. Let $\beta_i(\tilde{\varphi}(t)) \geq 0$, $\sum_{i=1}^{r} \beta_i(\tilde{\varphi}(t)) > 0$ for any $(\tilde{\varphi}(t))$. Hence $\lambda_i(\tilde{\varphi}(t))$ satisfies

$$\lambda_i(\tilde{\varphi}(x(t)) \geq 0 \text{ for } i \in \mathcal{I}, \text{ and } \sum_{i=1}^{r} \lambda_i(\tilde{\varphi}(x(t))) = 1.$$

The system (11) will be considered as the model to be controlled in the next section.

5 | FUZZY SAMPLED-DATA CONTROL

Only discrete $x(t)$ measurements can be used for sampled-data power, which means we only have measurements $x(t_k)$ at the sampling moment t_k. Utilizing zero-order hold (ZOH) with

$$0 = t_0 < t_1 < \cdots < t_k < \cdots$$

and $t_k \to \infty$ as $t \to \infty$. For $t \in [t_k, t_{k+1})$, the control signal has a constant value $u(t)$. Based on the facts provided above, the fuzzy sampled-data control is stated as follows:

Controller Rule j: **IF** $\tilde{\tilde{\varphi}}_1(t)$ is M_{j1}, $\tilde{\tilde{\varphi}}_2(t)$ is M_{j2}, $\cdots$, and $\tilde{\tilde{\varphi}}_p(t)$ is M_{jp}, **THEN**

$$u(t) = K_j x(t_k), \; t_k \leq t < t_{k+1}, \tag{12}$$

where K_j means the control gain matrices and t_k indicates the sampling instant and satisfies $\lim_{k\to\infty} t_k = +\infty$. The sampling intervals $t_k \le t < t_{k+1}$ are bounded such that $t_{k+1} - t_k = h_k \le h,\ k \ge 0$ and $t - t_k = h(t)$. Thus, we give the controller

$$u(t) = \sum_{j=1}^{r} \lambda_j(\tilde{\varphi}(t_k))K_j x(t_k). \tag{13}$$

Combining (13) with (11), we obtain

$$\begin{cases} \dot{x}(t) = \sum_{i=1}^{r}\sum_{j=1}^{r} \lambda_i(\varphi(t))\lambda_j(\varphi(t_k))\big[A_i x(t) + B_i K_j x(t_k) + B_w w(t)\big], \\ z(t) = \sum_{i=1}^{r} \lambda_i(\tilde{\varphi}(t))C_i x(t),\ i \in \mathcal{I}. \end{cases} \tag{14}$$

End of this section introduces the following Definition and Lemmas are utilized to get the main results:

Definition 1. [35] For the given matrices $\tilde{\chi}_1, \tilde{\chi}_2, \tilde{\chi}_3$ and $\tilde{\chi}_4$ satisfying $\tilde{\chi}_1 = \tilde{\chi}_1^T \le 0, \tilde{\chi}_3 = \tilde{\chi}_3^T > 0, \tilde{\chi}_4 = \tilde{\chi}_4^T \ge 0,\ \left(||\tilde{\chi}_1|| + ||\tilde{\chi}_2||\right).||\tilde{\chi}_4|| = 0$, the system (14) is said to be extended dissipative, if for any $\delta > 0$ such that, for all $t_f \ge 0$, the following inequality is satisfied with respect to the zero initial condition:

$$\int_0^{t_f} (z^T(t)\tilde{\chi}_1 z(t) + 2z^T(t)\tilde{\chi}_2 w(t) + w^T(t)\tilde{\chi}_3 w(t))dt \ge \sup_{0\le t\le t_f} y^T(t)\tilde{\chi}_4 y(t) + \delta. \tag{15}$$

Remark 1. The weighting matrices can be given values, and the principle of extended dissipativity can be used to find a general solution. (1) $\mathcal{L}_2 - \mathcal{L}_\infty$ performance: $\tilde{\chi}_1 = 0,\ \tilde{\chi}_2 = 0,\ \tilde{\chi}_3 = \tilde{\gamma}^2 I,\ \tilde{\chi}_4 = I$, and $\delta = 0$, (2) H_∞ performance: $\tilde{\chi}_1 = -I,\ \tilde{\chi}_2 = 0,\ \tilde{\chi}_3 = \tilde{\gamma}^2 I,\ \tilde{\chi}_4 = 0$, and $\delta = 0$, (3) Passivity performance: $\tilde{\chi}_1 = 0,\ \tilde{\chi}_2 = I,\ \tilde{\chi}_3 = \tilde{\gamma}, \tilde{\chi}_4 = 0$, and $\delta = 0$, (4) Mixed Passivity and $\mathcal{H}_\infty$ performance: $\tilde{\chi}_1 = \tilde{\gamma}^{-1}\alpha I,\ \tilde{\chi}_2 = (1-\alpha)I,\ \tilde{\chi}_3 = \tilde{\gamma} I,\ \tilde{\chi}_4 = 0$ and $\alpha = 0.4$, and (5) $(\tilde{\mathcal{Q}} - \tilde{\mathcal{S}} - \tilde{\mathcal{R}})$ Dissipativity: $\tilde{\chi}_1 = \tilde{\mathcal{Q}},\ \tilde{\chi}_2 = \tilde{\mathcal{S}},\ \tilde{\chi}_3 = \tilde{\mathcal{R}} - \tilde{\alpha} I$, and $\tilde{\chi}_4 = 0$.

Lemma 1. [15] For a given matrix $\mathcal{T} > 0$, the subsequent inequality holds for all continuously differential function x in $[\gamma_1, \gamma_2] \to \mathbb{R}^n$:

$$\int_{\gamma_1}^{\gamma_2} \dot{x}^T(s)\mathcal{T}\dot{x}(s)ds \ge \frac{1}{\gamma_2 - \gamma_1}\mathbb{V}_1^T(t)\mathcal{T}\mathbb{V}_1(t) + \frac{3}{\gamma_2 - \gamma_1}\mathbb{V}_2^T(t)\mathcal{T}\mathbb{V}_2(t)$$

where $\mathbb{V}_1(t) = x(\gamma_2) - x(\gamma_1),\ \mathbb{V}_2(t) = x(\gamma_2) + x(\gamma_1) - \frac{2}{\gamma_2-\gamma_1}\int_{\gamma_1}^{\gamma_2} x(s)ds$.

6 | MAIN RESULTS

In this part, we will focus on the extended dissipativity criterion for the system (14) as follows. Let us consider the following block matrices:

$$\Theta_{ij} = [A_i \quad B_i K_j \quad B_w \quad -I \quad 0],$$

and the corresponding block entry matrices as

$$\mathbb{E}_1 = [I\ 0\ 0\ 0\ 0]^T,\ \mathbb{E}_2 = [0\ I\ 0\ 0\ 0]^T,\ \mathbb{E}_3 = [0\ 0\ I\ 0\ 0]^T,\ \mathbb{E}_4 = [0\ 0\ 0\ I\ 0]^T,\ \mathbb{E}_5 = [0\ 0\ 0\ 0\ I]^T,$$
$$\xi^T(t) = \left[\, x^T(t)\ x^T(t_k)\ w^T(t)\ \dot{x}^T(t)\ \frac{2}{t-t_k}\int_{t_k}^{t} x^T(s)ds \,\right].$$

Theorem 1. Given gains $K_j,\ j \in \mathcal{I}$, scalars $h > 0, \gamma > 0$, and matrices $\tilde{\chi}_1, \tilde{\chi}_2, \tilde{\chi}_3, \tilde{\chi}_4$ the closed-loop system (14) is extended dissipative, if there exist matrix $P > 0,\ Q > 0$, matrices $Y, \mathbb{N}_1, \mathbb{N}_2, \mathbb{N}_3$, and $\mathbb{N}_4$ with adjustable dimensions such that the following LMIs are feasible with $h(t) = \{0, h\}$:

$$P - C^T\tilde{\chi}_4 C \ge 0, \tag{16}$$
$$\Psi_{ij} < 0,\ i, j \in \mathcal{I}, \tag{17}$$

where

$$\Psi_{ij} = \mathbb{E}_1^T P\mathbb{E}_4 + \mathbb{E}_4^T P^T\mathbb{E}_1 + h^2\mathbb{E}_4^T Q\mathbb{E}_4 + [\mathbb{E}_1^T Y + h(t)\mathbb{E}_2^T Y + \mathbb{E}_4^T Y]\Theta_{ij} + ([\mathbb{E}_1^T Y + h(t)\mathbb{E}_2^T Y + \mathbb{E}_4^T Y]\Theta_{ij})^T$$
$$- \mathbb{E}_1^T[C^T\tilde{\chi}_1 C]\mathbb{E}_1 - 2\mathbb{E}_1^T C^T\tilde{\chi}_2\mathbb{E}_3 - \mathbb{E}_3^T\tilde{\chi}_3\mathbb{E}_3 - (\mathbb{E}_1 - \mathbb{E}_2)^T Q(\mathbb{E}_1 - \mathbb{E}_2) - (\mathbb{E}_1 + \mathbb{E}_2 - \mathbb{E}_5)^T Q(\mathbb{E}_1 + \mathbb{E}_2 - \mathbb{E}_5).$$

Proof. Consider the following LKF candidate:

$$V(x_t) = x^T(t)Px(t) + h\int_h^0\int_{t+\theta}^t \dot{x}^T(s)Q\dot{x}(s)d\theta ds. \tag{18}$$

Now calculate the derivative of $V(x_t)$ along the trajectory of the system (14), we derive:

$$\dot{V}(x_t) = x^T(t)P\dot{x}(t) + \dot{x}^T(t)Px(t) + h^2\dot{x}^T(t)Q\dot{x}(t) - h\int_{t-h}^t \dot{x}^T(s)Q\dot{x}(s)ds,$$
$$\leq x^T(t)P\dot{x}(t) + \dot{x}^T(t)Px(t) + h^2\dot{x}^T(t)Q\dot{x}(t) - (t-t_k)\int_{t_k}^t \dot{x}^T(s)Q\dot{x}(s)ds. \tag{19}$$

Based on the Lemma 1, the above inequality in (19) becomes

$$-(t-t_k)\int_{t_k}^t \dot{x}^T(s)Q\dot{x}(s)ds \leq -\begin{bmatrix}\Gamma_1\\ \Gamma_2\end{bmatrix}^T\begin{bmatrix}Q & 0\\ 0 & 3Q\end{bmatrix}\begin{bmatrix}\Gamma_1\\ \Gamma_2\end{bmatrix},$$

where $\Gamma_1 = x(t) - x(t_k)$, $\Gamma_2 = x(t) + x(t_k) - \frac{2}{t-t_k}\int_{t_k}^t x(s)ds$.

According to system (14), for any adjustable dimension matrix Y, we have

$$= 2[x^T(t) + (t-t_k)x^T(t_k) + \dot{x}^T(t)]Y^T\left[-\dot{x}(t) + \sum_{i=1}^r\sum_{j=1}^r \lambda_i(x(t))\lambda_j(x(t_k))\left[A_i x(t) + B_i K_j x(t_k) + B_w w(t)\right]\right]. \tag{20}$$

Now, combining (19)–(20) and according to $J(t) = z^T(t)\tilde{\chi}_1 z(t) + z^T(t)\tilde{\chi}_2 w(t) + w^T(t)\tilde{\chi}_3 w(t)$, we get

$$\dot{V}(x_t) - J(t) \leq \sum_{i=1}^r\sum_{j=1}^r \lambda_i\lambda_j\xi^T(t)[\Sigma_{ij}]\xi(t) < 0. \tag{21}$$

Since $V(x_t)$ is continuous in t. Integrating (21) on both sides from t_0 to t, we have

$$\int_{t_0}^t J(s)ds \geq V(x_t) - V(x_{t_0}) \geq x^T(t)Px(t), \forall t \geq 0 \tag{22}$$

To meet Definition 1, we must demonstrate that the following inequality is true:

$$\int_{t_0}^{t_f} J(t)dt - \sup_{t_0\leq t\leq t_f} z^T(t)\tilde{\chi}_4 z(t) \geq 0, \tag{23}$$

First, choose $||\tilde{\chi}_4|| \neq 0$, it is obvious that following (22), we have

$$\int_{t_0}^{t_f} J(t)dt \geq 0.$$

Secondly, we choose that $||\tilde{\chi}_4|| > 0$. As stated in Assumption 1, the matrices in this situation as $\tilde{\chi}_1 = 0, \tilde{\chi}_2 = 0$ and $\tilde{\chi}_3 > 0$ and for any $t_0 \leq t \leq t_f$

$$\int_{t_0}^{t_f} J(s)ds \geq x^T(t)Px(t)$$
$$\geq x^T C^T \tilde{\chi}_4 Cx(t)$$
$$\geq z^T(t)\tilde{\chi}_4 z(t)$$
$$\dot{V}(x(t)) - J(t) \leq -\nu|\xi(t)|^2 \leq -\nu|x(t)|^2,$$
$$i.e., \dot{V}(x(t)) \leq J(t) - \nu|x(t)|^2.$$

Based on the preceding cases $||\tilde{\chi}_4|| = 0$ and $||\tilde{\chi}_4|| > 0$, the proposed closed-loop system (14) is extended dissipative for any non-zero $w(t) \in L_2[0, \infty)$ regarding Definition 1. Hence, we completed the proof. □

The sampled-data stabilization plan technique for fuzzy system (14) is given in the following theorem, which is based on Theorem 1.

Theorem 2. Given scalars $h > 0$, $\gamma > 0$, and matrices $\tilde{\chi}_1, \tilde{\chi}_2, \tilde{\chi}_3, \tilde{\chi}_4$, the fuzzy system (14) is extended dissipative, if there exist matrices $\overline{P} > 0$, $\overline{Q} > 0$, matrices $\overline{Y}$, and H_j with appropriate dimensions such that the following LMIs hold with $h(t) = \{0, h\}$:

$$P - C^T \tilde{\chi}_4 C \geq 0, \tag{24}$$

$$\overline{\Sigma}_{ij} = \begin{bmatrix} \overline{\Psi}_{ij} & \overline{Y}^T C^T \\ * & -\tilde{\chi}_1^{-1} I \end{bmatrix} < 0, \ i, j \in \mathcal{I}, \tag{25}$$

where

$$\overline{\Psi}_{ij} = \mathbb{E}_1^T \overline{P} \mathbb{E}_4 + \mathbb{E}_4^T \overline{P}^T \mathbb{E}_1 + h^2 \mathbb{E}_4^T \overline{Q} \mathbb{E}_4 + [\mathbb{E}_1^T Y + h(t)\mathbb{E}_2^T Y + \mathbb{E}_4^T Y]\Theta_{ij} + ([\mathbb{E}_1^T Y + h(t)\mathbb{E}_2^T Y + \mathbb{E}_4^T Y]\Theta_{ij})^T$$
$$- 2\mathbb{E}_1^T C^T \tilde{\chi}_2 \mathbb{E}_3 - \mathbb{E}_3^T \tilde{\chi}_3 \mathbb{E}_3 - (\mathbb{E}_1 - \mathbb{E}_2)^T \overline{Q}(\mathbb{E}_1 - \mathbb{E}_2) - (\mathbb{E}_1 + \mathbb{E}_2 - \mathbb{E}_5)^T \overline{Q}(\mathbb{E}_1 + \mathbb{E}_2 - \mathbb{E}_5).$$

The gain matrices K_j are given by $K_j = H_j \overline{Y}^{-1}$.

Proof. We calculate $\overline{\Sigma}_{ij} = \Pi^T \overline{\Sigma}_{ij} \Pi$, with $\Pi = diag\{\overline{Y}, \ \overline{Y}, \ I, \ \overline{Y}, \ \overline{Y}, \ I\}$, where $\overline{Y} = Y_j^{-1}, \ i \in \mathcal{I}$. Defining $\overline{P} = \overline{Y} P \overline{Y}$, $\overline{Q} = \overline{Y} Q \overline{Y}$.

The LMI (17) is pre- and post-multiplied by Π, as well as its transpose. After that, we can get LMIs (25). The proof is now complete. □

Remark 2. It merits referencing that SDC system can demonstrate numerous continuous time frameworks, for example, T-S fuzzy system, networks system models, digital frameworks, etc. Also, the benefits of utilizing SDC are minimal expense of control equipment, reliability and simple application. Recently, authors have been more attention on the research on wind energy conversation systems, PMSM system, PMSG system, and etc. To the best of author's knowledge, authors have not consider the bifurcation analysis for the PMSM system with the extended dissipatvity performance. Therefore, the results (Theorems and simulation) is much general and practical than [1,2,38,39].

7 | NUMERICAL SIMULATION AND ANALYSIS

The illustrative case has been provided in this section to represent the validity of the built-up theoretical findings using a sampled-data controller. To evaluate the simulation results, we consider two cases of PMSM study: without controller and with controller. For the first condition, the sampled data controller can generally be assumed as zero, caused by without disturbance. In the second study, this type of controller can be chosen by the gain matrix and show the performance of the effectiveness.

7.1 | Case Studys for PMSM without Controller:

The state responses of the PMSM framework dynamics are shown in FIGURES 7 -8 , respectively. When $u(t) = w(t) = 0$, an initial condition $x(0) = [-10, 10, 10, -10]^T$ and the chaotic behaviors are shown in FIGURES 7 -8 .

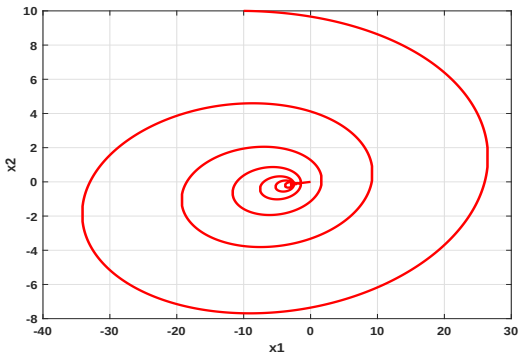

FIGURE 7 The chaotic x_1x_2 plane of PMSM.

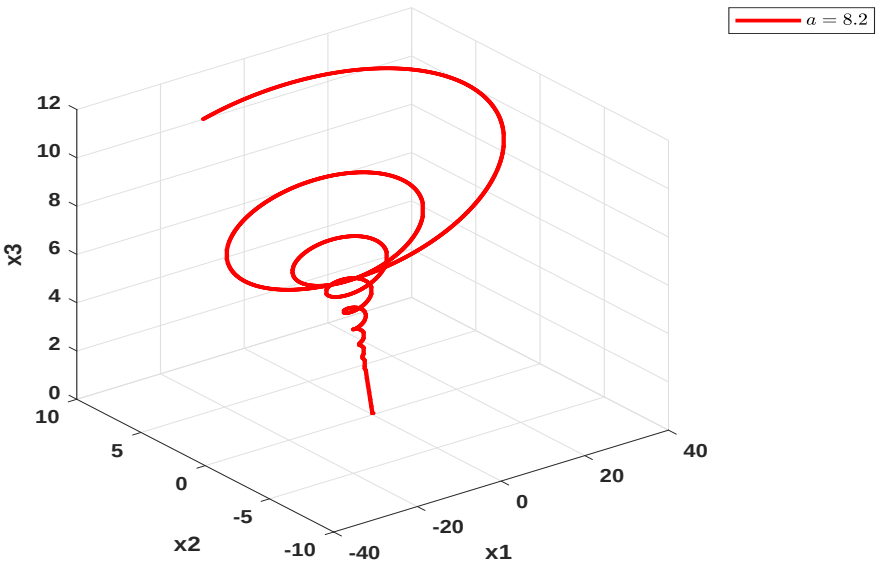

FIGURE 8 3D plane of PMSM.

7.2 | Case Studys for PMSM with Controller:

This section describes the feasibility and effectiveness of the new stability results and lists one example for the extend dissipative conditions. The input matrices and parameters are defined in (10) and TABLE 1.

$L_2 - L_\infty$ **performance:** Now, we consider $L_2 - L_\infty$ performance, the other cases can be similarly obtained. Choose the sampling period $h = 0.2$ and free weight matrix in the concept of extended dissipation as follows: Let $\tilde{\chi}_1 = 0$, $\tilde{\chi}_2 = 0$, $\tilde{\chi}_3 = \tilde{\gamma}^2 I$,

and $\tilde{\chi}_4 = I$. In addition, we choose the other parameters involved in the simulation are taken as in Table I. Use the Matlab LMI Control Toolbox to resolve LMIs (25) and feedback gain matrices

$$K_1 = \begin{bmatrix} -0.0131 & 0.0323 & -0.0001 & 0.0017 \\ 0.0082 & -0.0207 & 0.0331 & -0.0036 \end{bmatrix}, \; K_2 = \begin{bmatrix} -0.1681 & -1.2810 & 1.7455 & 0.0796 \\ -0.2602 & -1.7723 & -1.3377 & 0.3039 \end{bmatrix}.$$

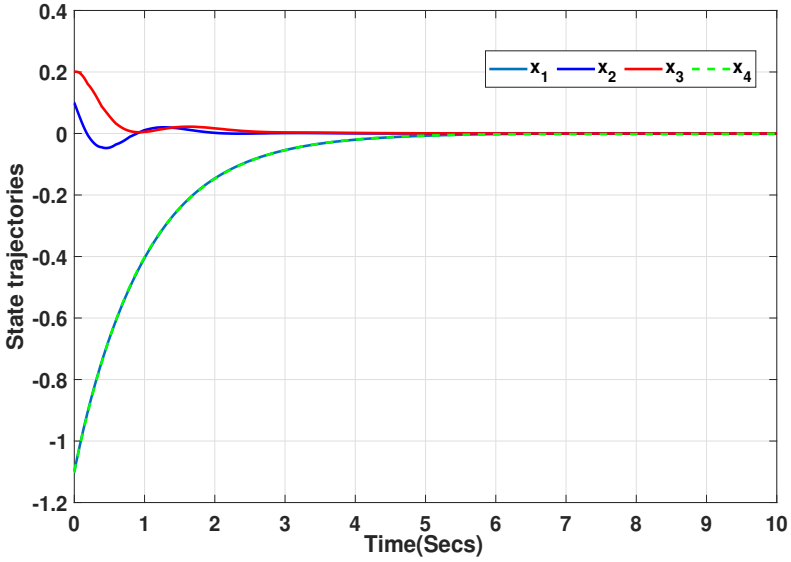

FIGURE 9 State response.

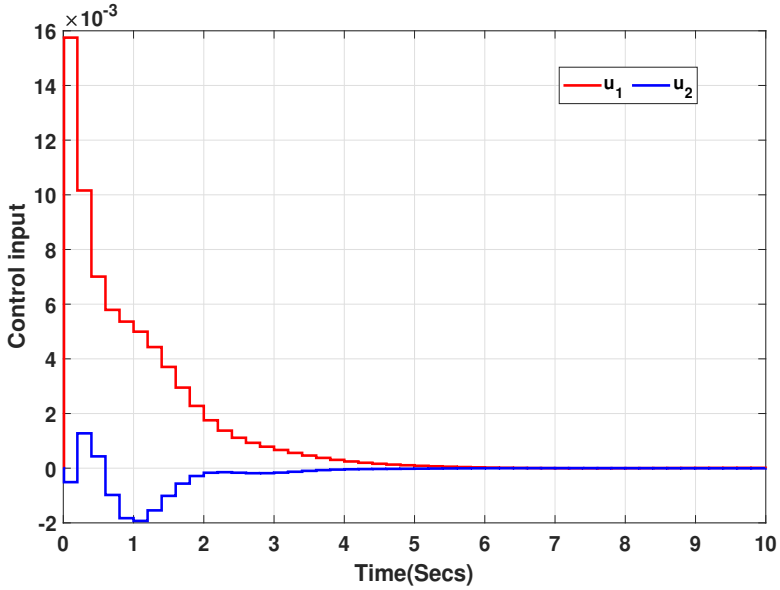

FIGURE 10 Control response.

TABLE 3 Four cases of the extended dissipative problems.

Analysis	$\tilde{\chi}_1$	$\tilde{\chi}_1$	$\tilde{\chi}_3$	$\tilde{\chi}_4$
$L_2 - L_\infty$ performance	0	0	γ^2 I	I
H_∞ performance	-I	0	γ^2 I	0
Passivity performance	0	I	γ^2 I	0
Dissipativity performance	-I	I	γ^2 I	0

TABLE 4 Control gain matrices for different performance in Table III.

Analysis	Control gain matrices
H_∞ performance	$K_1 = \begin{bmatrix} -0.1482 & -3.0937 & 2.6211 & 0.0524 \\ -0.4669 & -2.6465 & -3.2991 & 0.0434 \end{bmatrix}$ $K_2 = \begin{bmatrix} -0.4305 & -4.0731 & 0.4508 & 0.0580 \\ -0.2969 & -0.3719 & -4.3794 & 0.0107 \end{bmatrix}$.
Passivity performance	$K_1 = \begin{bmatrix} -0.1791 & -3.0591 & 2.6185 & 0.0838 \\ 0.1096 & -2.7059 & -3.3549 & 0.0677 \end{bmatrix}$ $K_2 = \begin{bmatrix} -0.0928 & -4.0682 & 0.3737 & 0.0914 \\ 0.1647 & -0.3690 & -4.4218 & 0.0156 \end{bmatrix}$.
Dissipativity performance	$K_1 = \begin{bmatrix} -0.1293 & -24.1198 & 9.1775 & 0.0479 \\ 0.1903 & -10.5570 & -26.9011 & 0.0317 \end{bmatrix}$ $K_2 = \begin{bmatrix} -0.1375 & -25.3935 & -0.0128 & 0.0497 \\ 0.2304 & 0.1148 & -27.6836 & 0.0039 \end{bmatrix}$.

The state and control response of the PMSM system is shown in FIGURES 9 -10 . From Remark 1, we know that by setting different values of $\tilde{\chi}_1$, $\tilde{\chi}_2$, $\tilde{\chi}_3$ and $\tilde{\chi}_4$, the extended dissipative performance can be turned into four different performances, which are shown in TABLE 3. Moreover, initiate the sampling period $h = 0.2$ and by solving LMIs in Theorem 2, we get the related controller matrices, which are shown in TABLE 3.

It is concluded from the simulation results that good performances are achieved for the PMSM model under the condition of the sampled data controller. The extended dissipative performances and other constraints are satisfied with the proposed controller.

Moreover, none of the above mentioned studies on PMSM system have solved the problem of extended dissipative conditions. Therefore, the method developed in this study is more general and effective.

8 | CONCLUSIONS

In this article, we investigated the bifurcation analysis and Takagi-Sugeno fuzzy sampled-data control of PMSM's model. The system's physical plant was defined as an average weighted sum of local linear subsystems, with membership functions defining the weighting terms. On the basis of the LKF strategy, a free weighting matrix procedure, a novel effective inequality technique, and some adequate conditions in the way of LMIs have been obtained, ensuring that the scheme is expanded dissipative and reduces the conservatism of the established findings. Then, by solving the group of LMIs, the necessary sampled-data fuzzy controller gains can be obtained. Numerical examples have been used to demonstrate the benefit and feasibility of the proposed controller design scheme. As a result, in order to conserve computing resources, we could explore more complex systems in the

future, such as semi-Markov model-based stochastic nonlinear systems and distributed event-triggered performance feedback controllers.

References

1. Li Zhong, Park Jin Bae, Joo Young Hoon, Zhang Bo, Chen Guanrong. Bifurcations and chaos in a permanent-magnet synchronous motor. *IEEE Transactions on Circuits and Systems I: Fundamental Theory and Applications.* 2002;49(3):383–387.

2. Jung J-W, Choi Y-S, Leu VQ, Choi HH. Fuzzy PI-type current controllers for permanent magnet synchronous motors. *IET electric power applications.* 2011;5(1):143–152.

3. Bistak S, Kim S. AC Induction Motors vs. Permanent Magnet Synchronous Motors. *Fuji Electric Corp of America.* 2017;.

4. Vu Nga Thi-Thuy, Yu Dong-Young, Choi Han Ho, Jung Jin-Woo. T–S fuzzy-model-based sliding-mode control for surface-mounted permanent-magnet synchronous motors considering uncertainties. *IEEE Transactions on Industrial Electronics.* 2012;60(10):4281–4291.

5. Guo Shenghui, Zhu Fanglai, Zhang Wei, Żak Stanisław H, Zhang Jian. Fault detection and reconstruction for discrete nonlinear systems via Takagi-Sugeno fuzzy models. *International Journal of Control, Automation and Systems.* 2018;16(6):2676–2687.

6. Taniguchi Tadanari, Tanaka Kazuo, Ohtake Hiroshi, Wang Hua O. Model construction, rule reduction, and robust compensation for generalized form of Takagi-Sugeno fuzzy systems. *IEEE Transactions on Fuzzy Systems.* 2001;9(4):525–538.

7. Zhou Jianzhong, Zhang Nan, Li Chaoshun, Zhang Yongchuan, Lai Xinjie. An Adaptive Takagi–Sugeno Fuzzy Model-Based Generalized Predictive Controller for Pumped-Storage Unit. *IEEE Access.* 2019;7:103538–103555.

8. Zhu Xiaoyuan, Li Wei. Takagi–Sugeno fuzzy model based shaft torque estimation for integrated motor–transmission system. *ISA Transactions.* 2019;93:14–22.

9. Yang Huilan, Shu Lan, Wang Xin, Zhong Shouming. Synchronization of IT2 stochastic fuzzy complex dynamical networks with time-varying delay via fuzzy pinning control. *Journal of the Franklin Institute.* 2019;356(3):1484–1501.

10. Gunasekaran Nallappan, Saravanakumar Ramasamy, Joo Young Hoon, Kim Han Sol. Finite-time synchronization of sampled-data T–S fuzzy complex dynamical networks subject to average dwell-time approach. *Fuzzy Sets and Systems.* 2019;374:40–59.

11. Wen Yao, Chang Hongbin, Su Xiaojie, Assawinchaichote Wudhichai. Event-triggered fuzzy control of repeated scalar nonlinear systems and its application to chua's circuit system. *IEEE Transactions on Circuits and Systems I: Regular Papers.* 2020;.

12. Xia Yude, Wang Jing, Meng Bo, Chen Xiangyong. Further results on fuzzy sampled-data stabilization of chaotic nonlinear systems. *Applied Mathematics and Computation.* 2020;379:125225.

13. Kim Han Sol, Lee Kwangil. Design of a fault tolerant sampled-data fuzzy observer with exponential time-varying gains. *IEEE Access.* 2020;8:68488–68498.

14. Wang Zi-Peng, Wu Huai-Ning, Chadli Mohammed. H_∞ sampled-data fuzzy observer design for nonlinear parabolic PDE systems. *IEEE Transactions on Fuzzy Systems.* 2020;.

15. Zhang Chuan-Ke, He Yong, Jiang Lin, Lin Wen-Juan, Wu Min. Delay-dependent stability analysis of neural networks with time-varying delay: A generalized free-weighting-matrix approach. *Applied Mathematics and Computation.* 2017;294:102–120.

16. Chang Yufang, Zhai Guisheng, Fu Bo, Xiong Lianglin. Quadratic stabilization of switched uncertain linear systems: a convex combination approach. *IEEE/CAA Journal of Automatica Sinica.* 2019;6(5):1116–1126.

17. Xiang Weiming, Zhai Guisheng, Briat Corentin. Stability analysis for LTI control systems with controller failures and its application in failure tolerant control. *IEEE Transactions on Automatic Control.* 2015;61(3):811–816.

18. Mao Yanbing, Zhang Hongbin, Xu Shengyuan. The exponential stability and asynchronous stabilization of a class of switched nonlinear system via the T–S fuzzy model. *IEEE Transactions on Fuzzy Systems.* 2013;22(4):817–828.

19. Gunasekaran Nallappan, Joo Young Hoon. Robust sampled-data fuzzy control for nonlinear systems and its applications: Free-weight matrix method. *IEEE Transactions on Fuzzy Systems.* 2019;27(11):2130–2139.

20. Mao Jun, Xiang Zhengrong, Zhai Guisheng. Global practical stabilisation of a class of switched nonlinear systems via sampled-data control. *International Journal of Control.* 2020;93(8):1891–1906.

21. Gunasekaran Nallappan, Zhai Guisheng, Yu Qiang. Sampled-data synchronization of delayed multi-agent networks and its application to coupled circuit. *Neurocomputing.* 2020;413:499–511.

22. Mao Jun, Xiang Zhengrong, Zhai Guisheng. Sampled-data control of a class of switched nonlinear systems under asynchronous switching. *Journal of the Franklin Institute.* 2019;356(4):1924–1943.

23. Theesar S Jeeva Sathya, Balasubramaniam P. Secure communication via synchronization of Lur'e systems using sampled-data controller. *Circuits, Systems, and Signal Processing.* 2014;33(1):37–52.

24. Guo Shu-Mei, Shieh Leang S, Chen Guanrong, Ortega Maritza. Ordering chaos in Chua's circuit: A sampled-data feedback and digital redesign approach. *International Journal of Bifurcation and Chaos.* 2000;10(09):2221–2231.

25. Shanmugam Lakshmanan, Joo Young Hoon. Design of interval type-2 fuzzy-based sampled-data controller for nonlinear systems using novel fuzzy Lyapunov functional and its application to PMSM. *IEEE Transactions on Systems, Man, and Cybernetics: Systems.* 2018;.

26. Zheng Minjie, Yang Shenhua, Li Lina. Stability Analysis and TS Fuzzy Dynamic Positioning Controller Design for Autonomous Surface Vehicles Based on Sampled-Data Control. *IEEE Access.* 2020;8:148193–148202.

27. Li Hongyi, Jing Xingjian, Lam Hak-Keung, Shi Peng. Fuzzy sampled-data control for uncertain vehicle suspension systems. *IEEE transactions on cybernetics.* 2013;44(7):1111–1126.

28. Gunasekaran Nallappan, Joo Young Hoon. Stochastic sampled-data controller for T–S fuzzy chaotic systems and its applications. *IET Control Theory & Applications.* 2019;13(12):1834–1843.

29. Zhao Jianrong, Xu Shengyuan, Park Ju H. Improved criteria for the stabilization of TS fuzzy systems with actuator failures via a sampled-data fuzzy controller. *Fuzzy Sets and Systems.* 2020;392:154–169.

30. Wang Zi-Peng, Wu Huai-Ning, Huang Tingwen. Sampled-data fuzzy control for nonlinear delayed distributed parameter systems. *IEEE Transactions on Fuzzy Systems.* 2020;.

31. Zhang Ruimei, Zeng Deqiang, Park Ju H, Lam Hak-Keung, Xie Xiangpeng. Fuzzy sampled-data control for synchronization of T-S fuzzy reaction-diffusion neural networks With additive time-varying delays. *IEEE Transactions on Cybernetics.* 2020;.

32. Willems Jan C. Dissipative dynamical systems part I: General theory. *Archive for Rational Mechanics and Analysis.* 1972;45(5):321–351.

33. Hill David J, Moylan Peter J. Dissipative dynamical systems: Basic input-output and state properties. *Journal of the Franklin Institute.* 1980;309(5):327–357.

34. Brogliato Bernard, Lozano Rogelio, Maschke Bernhard, Egeland Olav. Dissipative systems analysis and control. *Theory and Applications.* 2007;2.

35. Wei Hongzhi, Li Ruoxia, Chen Chunrong, Tu Zhengwen. Extended dissipative analysis for memristive neural networks with two additive time-varying delay components. *Neurocomputing.* 2016;216:429–438.

36. Vadivel Rajarathinam, Joo Young Hoon. Finite-time sampled-data fuzzy control for a non-linear system using passivity and passification approaches and its application. *IET Control Theory & Applications.* 2020;14(8):1033–1045.

37. Gunasekaran Nallappan, Saravanakumar Ramasamy, Syed Ali M, Zhu Quanxin. Exponential sampled-data control for T–S fuzzy systems: application to Chua's circuit. *International Journal of Systems Science.* 2019;50(16):2979–2992.

38. Vadivel R., Joo Young Hoon. Reliable Fuzzy H Control for Permanent Magnet Synchronous Motor Against Stochastic Actuator Faults. *IEEE Transactions on Systems, Man, and Cybernetics: Systems.* 2021;51(4):2232-2245.

39. Gunasekaran Nallappan, Joo Young Hoon. Nie–Tan fuzzy method of fault-tolerant wind energy conversion systems via sampled-data control. *IET Control Theory & Applications.* 2020;14(11):1516–1523.

40. Chang Yuan-Chih, Chen Chien-Hua, Zhu Zhong-Chuan, Huang Yi-Wen. Speed control of the surface-mounted permanent-magnet synchronous motor based on Takagi–Sugeno fuzzy models. *IEEE Transactions on Power Electronics.* 2015;31(9):6504–6510.